J. Fluid Mech. (1979), *vol.* 93, *part* 3, *pp.* 465–489
Printed in Great Britain

Experimental study of wall shear rates in the entry region of a curved tube

By U. S. CHOI, L. TALBOT AND I. CORNET
Department of Mechanical Engineering, University of California, Berkeley

(Received 15 August 1978 and in revised form 22 November 1978)

Local wall shear rates in steady flow in the entry region of a curved tube have been measured by the electrochemical limiting current method. A semi-circular rigid tube of circular cross-section with radius ratio $\frac{1}{7}$ has been employed for a range of Dean number between 139 and 2868. The circumferential and axial distributions of the wall shear rates have been measured at 20° circumferential increments at five different sections of the entry region.

The experimental wall shear distributions show a valley in the circumferential wall shear profile and a region of non-monotonic variation of the average wall shear rates with downstream distance, both of which are prominent features of the entry flow in a curved tube. The existence of the valley suggests a vortex structure with several pairs of vortices in a developing curved tube flow in contrast with one pair in a fully developed flow. The circumferential distribution of wall shear also suggest that a potential vortex flow is formed in the upstream core. The wall shear is lowest at the innermost part of the bend and reaches a maximum in the mid-circumference region. The wall shear is significantly enhanced by secondary flows, as much as eight times greater in the curved tube entry flow than in fully developed Poiseuille flow in the range of Dean number between 139 and 2868. The cross-over in shear maximum from the inner part of the bend to the outer part occurs at about 1·9 cross-section radii from the inlet and seems to decrease with Dean number.

1. Introduction

A knowledge of flow and wall shear or mass transfer in curved tubes is of importance in developing a realistic mathematical model for curved tube flow. It is also of practical importance in many branches of engineering. For example, information on the increase in resistance due to curvature is necessary in determining pumping power, and the enhanced convective heat transfer due to secondary flow is important in the design of heating and cooling coils used in heat exchangers and refrigeration equipment, especially in heat exchangers in nuclear reactors. Entry flows in a curved tube have recently become of considerable concern to physiologists because the effects of fluid dynamics are considered to play an important role in the circulatory system. Much emphasis has been placed upon precise distributions of flow velocity or of rates of shear and mass transport in connexion with the blood flow in the aortic arch, particularly as they might relate to the formation of atherosclerotic plaques on the vascular wall resulting from atheromatous deposits (Lighthill 1972). There are many theories which attempt to explain the occurrence of the deposits in terms of fluid mechanics.

0022–1120/79/4240–6780 $02.00

For example, Fry (1968, 1973) suggests that atheromatous lesions may occur in areas where the wall shear stress is greatest. An opposite view has been advanced by Caro, Fitz-Gerald & Schroter (1971) who suggest a close correspondence between areas of atherogenesis and areas of low shear and mass transport rates. The arguments regarding the correlation between wall shear and mass transport rates and incipient atheroma are rather qualitative and there are still controversies about the effect of high shear and low shear stresses. There is, in fact, little knowledge of the nature and effect of the flow in the entry region of a curved tube. Also, no experimental studies have to our knowledge been carried out on local shear rates in the entry region of a curved tube. Therefore quantitative information on shear in the entry region of a curved tube is of considerable interest, and the purpose of the present study is to provide the characteristics of the entry flow in a curved tube by experimental measurements of local wall shear rates using an electrochemical limiting current method.

2. Previous investigations

Many investigations, both theoretical and experimental, have been carried out on fully developed flow in curved tubes since the pioneering work of Dean (1927, 1928). A good summary is given by Collins & Dennis (1975). Dean was the first to obtain a quantitative description of the two counter-rotating secondary flow vortices characteristic of fully developed flow in a curved pipe. He showed that dynamical similarity of the flow depends on the parameter $\kappa' = (a/R)^{\frac{1}{2}}(2u_0 a/\nu)$ where a is the pipe radius, R its radius of curvature, ν the kinematic viscosity, and u_0 the mean axial velocity which would obtain in a straight pipe under the same imposed pressure gradient. κ' is often referred to as the Dean number. For experimental purposes, a more convenient parameter is $\kappa = (a/R)^{\frac{1}{2}}(2\bar{u}a/\nu)$, where $\bar{u}$ is the mean axial velocity in the curved pipe, and in the present work κ will be referred to as the Dean number.

There have been relatively few investigations of the entry flow region of a curved pipe and the way in which the Dean-type motion develops. Hawthorne (1951) and Smith (1976) studied the process of transition from Poiseuille flow in a straight tube to fully developed curved tube flow, and Humphrey (1977) carried out a numerical analysis of Poiseuille flow passing through a 90° bend. The case of uniform velocity at the entrance to a curved tube is of particular interest because of its relevance to aortic flow. This case has been investigated analytically by Singh (1974) and Yao & Berger (1975). Patankar, Pratap & Spalding (1974) carried out a numerical study of both the hydrodynamic and thermal entry flow for helically coiled tubes. Some of these investigations will be referred to subsequently.

On the experimental side, the only investigation of flow into a curved pipe with uniform entry conditions which is available to us is the laser-Doppler-velocimeter measurement of the axial and secondary velocity components by Agrawal, Talbot & Gong (1978), although measurements by Olson (1971) are mentioned by Singh.

Agrawal *et al.* give an interesting description of the entry flow development in terms of the generation of streamwise vorticity. Their velocity data can be used to infer local wall shear values by extrapolation; however this is not a very accurate procedure and it is desirable to obtain shear values by direct measurements, such as is provided by the electrochemical method. Before proceeding to the description of the experiment, a brief review of the method will be given.

3. Experiments

3.1. *The electrochemical method*

The electrochemical method as applied to heat and mass transfer problems has been reviewed by Mizushina (1971), and only a very brief description of the technique as it pertains to the present work will be given here.

In a typical application of the method, an electrolytic reaction is caused to occur between two nickel electrodes, a small nickel cathode mounted flush with the wall at the point of measurement, and a large anode mounted downstream. If the electrolyte is chosen to be an equimolar concentration of potassium ferro- and ferri-cyanides (0·1 molar in the present case) mixed with an excess of supporting electrolyte (1·0 molar of sodium hydroxide in the present case), then under the application of a d.c. potential between the electrodes the following reversible reactions occur. At the cathode

$$\underset{\text{(ferricyanide)}}{Fe(CN_6)^{3-}} + e \rightarrow \underset{\text{(ferrocyanide)}}{Fe(CN_6)^{4-}} \quad \text{(reduction reaction)};$$

while at the anode

$$Fe(CN_6)^{4-} \rightarrow Fe\ (CN_6)^{3-} + e \quad \text{(oxidation reaction)}.$$

It can be shown that because of the presence of the supporting electrolyte, the current which flows between the electrodes in this redox reaction is due almost entirely to concentration diffusion of the carrier ions. Thus, under steady state conditions, the flux $\dot{N}$ of ferricyanide ions per unit area to the cathode is given by

$$\dot{N} = D\left(\frac{\partial C}{\partial y}\right)_w, \tag{1}$$

where C is the concentration of the ferricyanide ion and D its diffusion coefficient. (An identical relation holds for the ferrocyanide ion at the anode, but it is not of concern to us.) The total measured current I is related to the flux $\dot{N}$ by Faraday's first law (assuming an ion valence charge of unity),

$$\dot{N}(= I/AF), \tag{2}$$

where A is the area of the test electrode and F is Faraday's constant (= 96494 coulombs per equivalent). If we define a mass transfer coefficient k such that

$$k = \frac{\dot{N}}{C_\infty - C_w}, \tag{3}$$

where C_∞ is the bulk concentration of the ferricyanide ion and C_w its concentration at the wall, then we have

$$k = \frac{D(\partial C/\partial y)_w}{C_\infty - C_w} = \frac{I}{AF(C_\infty - C_w)}. \tag{4}$$

The essence of the limiting-current technique is to increase the potential between the electrodes until the diffusion-limited current is reached, which corresponds to reducing the wall concentration to zero, and thus

$$k = \frac{D(\partial C/\partial y)_w}{C_\infty} = \frac{I_L}{AFC_\infty}, \tag{5}$$

where I_L is the ionic mass transfer limiting current at which reduction of the ferricyanide ion is achieved at maximum rate. Since C_∞ and D are presumed known, the measurement of I_L determines the wall concentration gradient $(\partial C/\partial y)_w$.

Our objective is to relate the wall concentration gradient to the wall shear stress. Because the Schmidt number $Sc = \nu/D$ is large (in the present experiments, with kinematic viscosity $\nu = 1{\cdot}064 \times 10^{-2}$ cm^2/s, and $D = 6{\cdot}33 \times 10^{-6}$ cm^2/s, $Sc = 1680$), the concentration boundary layer adjacent to the electrode is much thinner than the velocity boundary layer, analogous to the comparative thickness of the thermal boundary layer in the large Prandtl number limit. The governing equation for steady mass transfer between a fluid flow and a bounding surface in the boundary layer approximation is

$$u\frac{\partial C}{\partial x} + v\frac{\partial C}{\partial y} = D\frac{\partial^2 C}{\partial y^2}, \tag{6}$$

where u and v are the flow velocities in the x and y directions, parallel to the surface and normal to it. In the limit of $Sc \gg 1$, the velocity profile within the concentration boundary layer can be approximated by

$$u \doteq \frac{\tau_w}{\mu} y \equiv \beta(x)\, y$$

and

$$v = -(y^2/2)\,(d\beta/dx) \quad \text{(from continuity)}, \tag{7}$$

where τ_w is the wall shear, $\mu = \nu\rho$ the viscosity, and $\beta(x) \equiv \tau_w/\mu$ the wall velocity gradient, which can be a function of x. The boundary conditions of interest to us are $C = C_\infty$ at $y = \infty$, $C = 0$ at $y = 0$.

Lighthill (1950) has solved the analogous heat transfer problem. His result, when expressed in mass transfer terms, is

$$\frac{kC_\infty}{D} = \left(\frac{\partial C}{\partial y}\right)_w = \frac{C_\infty(\beta(x))^{\frac{1}{2}}}{\Gamma(\frac{4}{3})\left[9D\int_0^x (\beta(t))^{\frac{1}{2}}\,dt\right]^{\frac{1}{3}}}. \tag{8}$$

If $\beta = \bar{\beta}$, independent of x (a reasonable approximation for a small isolated electrode), then this reduces to the classical Lévêque (1928) solution,

$$\bar{\beta} = \frac{\tau_w}{\mu} = \frac{1{\cdot}8989k^3L}{D^2}, \tag{9}$$

where L is the distance from the leading edge to the trailing edge of the wall region over which mass transfer occurs. In the case of an isolated circular electrode of diameter d_e flush with the wall, $L = 0{\cdot}8136d_e$ (Mizushina 1971, p. 139).

Equation (9) provides us with the necessary result. Since k is determined from the measurement of the limiting current, I_L, according to (5), and all other quantities are known, the local wall shear is determined.

3.2. *Experimental apparatus and procedure*

A schematic representation of the flow system used in the present study appears in figure 1. A steady flow was supplied by a header tank. The fluid level in this tank was kept constant by continuously pumping in fluid from a receiving tank and by letting

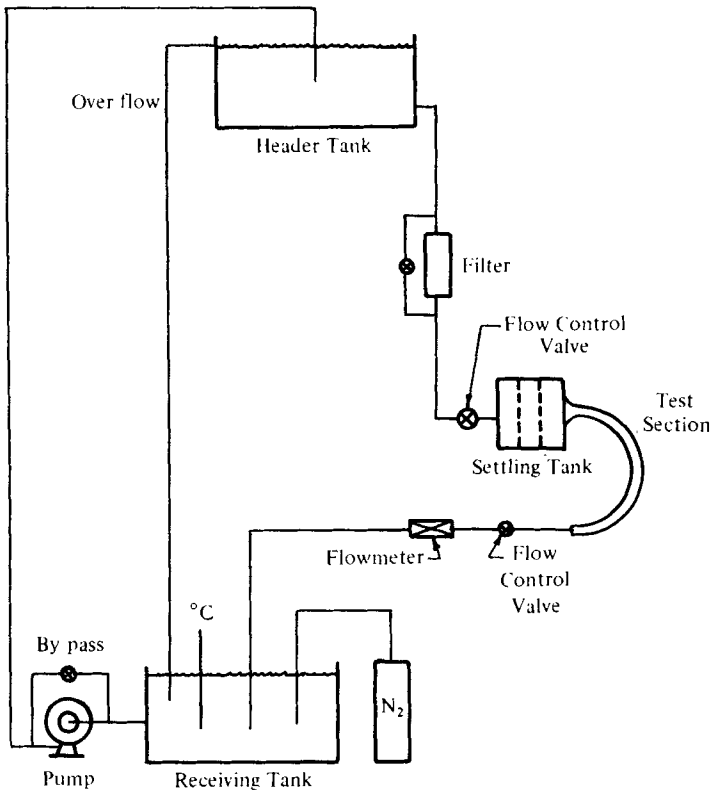

FIGURE 1. The flow system.

the overflow flow back into the receiving tank. An 'intercept' blood transfusion filter was introduced in the pump circuit to remove all undesirable debris over 20 μm in size and to remove gas bubbles in suspension. The flow rate through the test section was controlled by flow control valves. The electrolyte solution entered from a constant-head tank via a bellmouth settling tank into the test section having a circular cross section of diameter 3·81 cm. A multiple orifice plate and two sets of screens inside the settling tank served to reduce velocity variations and damp large eddies created by the flow from the header tank located approximately 2 m above the test section. Thus the velocity profiles at entry to the test section were laminar and almost uniform. This entry condition for simulating aortic flow is well justified by Bellhouse & Talbot (1969). The entire flow system was wrapped with aluminium foil to prevent decomposition of the solution by light.

Curved tube and straight tube test sections were fabricated of Lucite plastic. A semicircular tube test section of diameter 3·81 cm and radius ratio $a/R = \frac{1}{7}$ was employed for study of curved tube flow and a straight tube test section was used in place of the semicircular tube test section for study of entry flow in a straight tube. Each test section was machined in two halves from plastic sheet and joined together at the plane of symmetry.

Test electrodes were mounted flush with the local surface of the test section at five sections along the tube axis as shown in figure 2. At each section eight electrodes

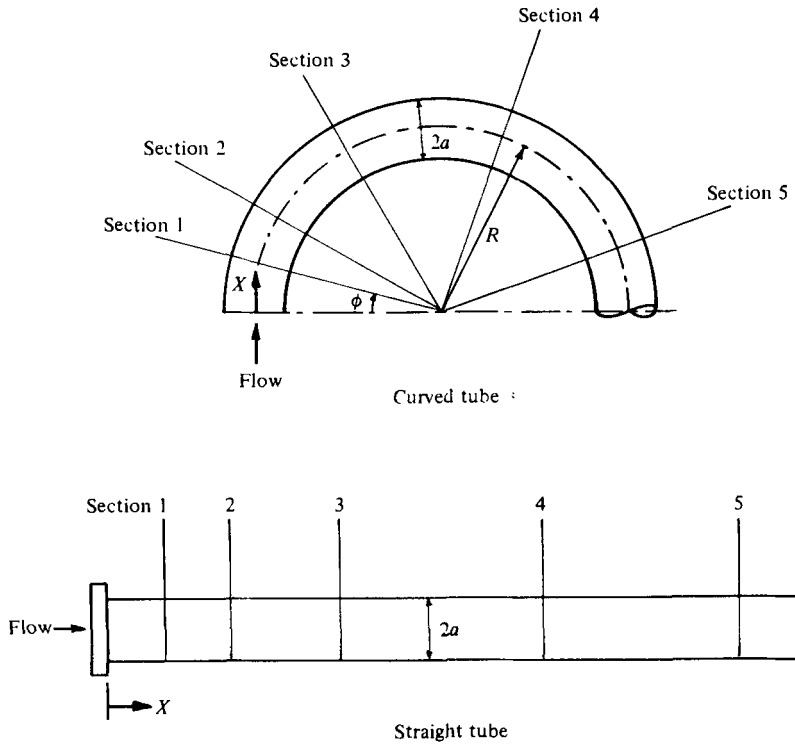

FIGURE 2. Test sections.

Section	ϕ (deg)	X (cm)	X/a
1	15	3·49	1·84
2	30	6·99	3·68
3	60	13·97	7·34
4	110	25·60	13·44
5	160	37·24	19·54

were equispaced around the circumference as shown in figure 3. The probes were imbedded only on the lower half surface of the test section because it was desired to avoid bubble attachment to the electrodes. All test electrodes were made of 99·97 % pure nickel wire of diameter 0·1587 cm. The lateral surfaces of the electrodes were coated with 'Kynar' resin. The anode was made of a nickel cylinder of diameter 2·54 cm and of length 7·62 cm, and was installed in the discharge line immediately downstream of the test section.

The completely assembled test section with all probes installed was connected to the contraction section of the settling tank and the outlet end of the test section was fitted to 2·54 cm acrylic tubing through a moderate contraction. For calibration of the experimental system a straight tube test section was connected downstream of a straight tube of sufficient length to ensure that the velocity profile at entry to the straight tube test section was fully developed throughout the range of Reynolds numbers encountered in the tests.

A potentiostat was designed to apply a potential to all cathodes simultaneously and to keep the potential across the electrodes at a fixed value. The current flowing

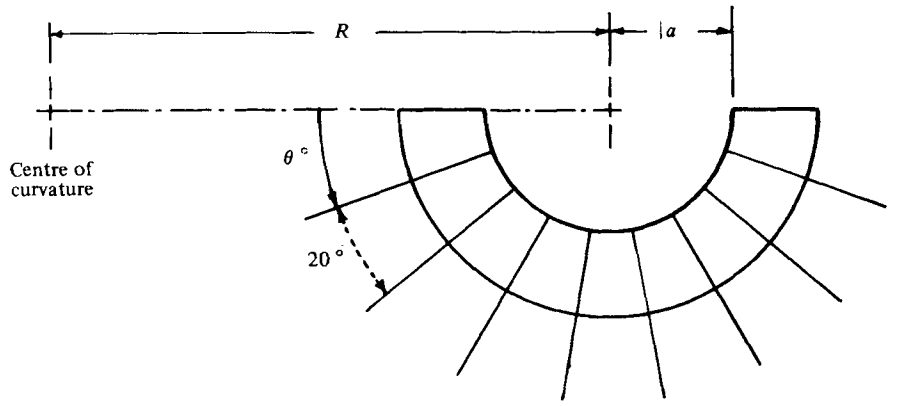

FIGURE 3. Positions of test electrodes at each section.
Electrode diameter = 0·1587 cm.

through each of the individual cathodes was determined by setting the forty-position switch of the potentiostat at a position corresponding to a particular cathode and by measuring the voltage drop across a precision resistor in the metering circuit.

The flow rate was measured by an electromagnetic flowmeter. It was calibrated using a bucket and stopwatch before running a test.

A chromel-alumel thermocouple in the receiving tank was used to measure the temperature of the solution during the experiments. No attempt was made to maintain the solution at a constant temperature. It was found to be unnecessary because the fluctuations of the temperature from 25 °C were small.

The electrolyte consisted of AR grade potassium ferricyanide of 0·01 M, ferrocyanide of 0·01 M, and sodium hydroxide of 1·0 M, dissolved in de-ionized water. The relevant physical properties of the solution are the ferricyanide ion concentration, and the density, viscosity and diffusivity of the solution. The property values for the electrolyte were calculated using semi-empirical equations given by Gordon, Newman & Tobias (1965).

The solution was purged with nitrogen to remove dissolved oxygen for more than one hour before making a run and purging was continued during the experiments. Before each experimental run the electrode surfaces were polished with fine sand paper, buffed and rinsed with distilled water; the anode was treated in the same way. All electrodes were treated cathodically in a 5% NaOH solution, before the test section was installed in the flow circuit.

When the desired flow condition was established, a voltage was applied simultaneously to all test electrodes and increased incrementally up to about 1·0 V and the current passing through each electrode was recorded after each increment. A plot of voltage *vs.* current was constructed to obtain the limiting current for each electrode, from which the wall shear was determined as described earlier.

Further details of the apparatus and procedure can be found in the report by Choi (1978).

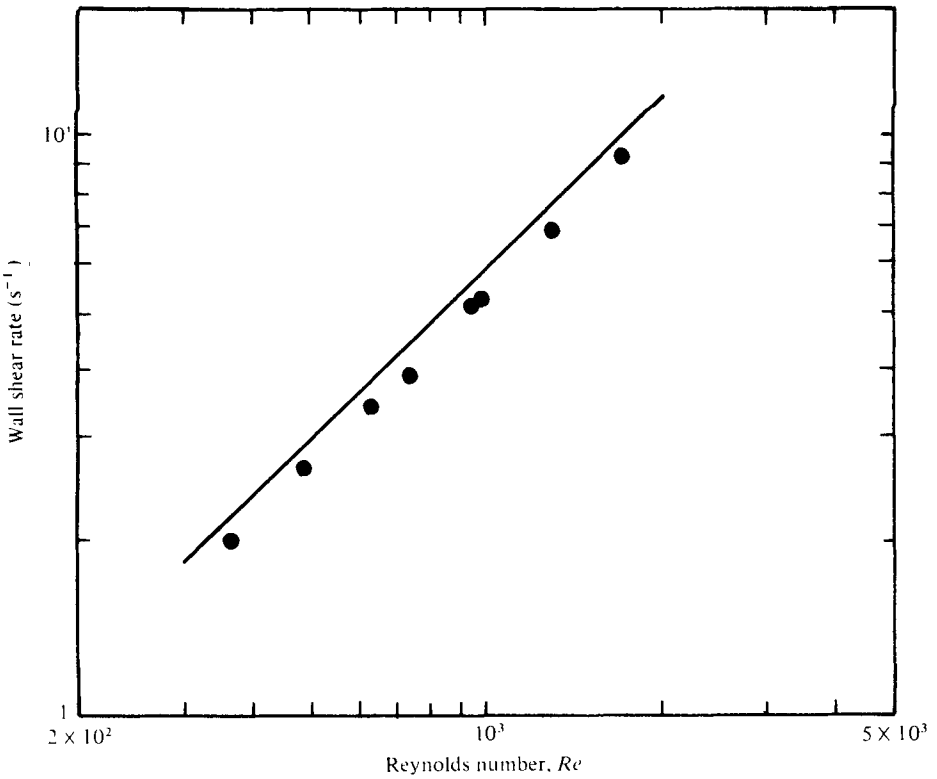

FIGURE 4. Steady calibration in Poiseuille flow. ●, experimental; —, theoretical.

4. Results and discussion

4.1. *Calibration of probes in a straight tube*

To test the accuracy of the experimental method, calibration measurements were performed in a fully developed laminar flow in a straight tube. A straight tube test section was connected 70 diameters downstream from entry where the velocity profile at the test section was at least 98 % developed (Langhaar 1942) for all calibration flow rates ($Re = 2\bar{u}a/\nu = 366$ to 1701). A typical steady calibration curve is shown in figure 4. The theoretical wall shear rate for Poiseuille flow is

$$\bar{\beta} = \frac{2\nu}{a^2} Re \tag{10}$$

and this is represented by the theoretical line in figure 4.

It is noted that the experimental data fall on a straight line but are consistently lower than theoretical values calculated from (10) by approximately 7 %. The reason for this discrepancy is not known.

A straight tube test section was joined directly with the contraction section of the settling tank in order to examine the comparison between theory and experiment for entry flow in a straight tube, thus providing another form of electrode calibration. The experimental data is shown in figure 5. Comparison of the experimental data with Langhaar's theoretical predictions shows good agreement although the experimental

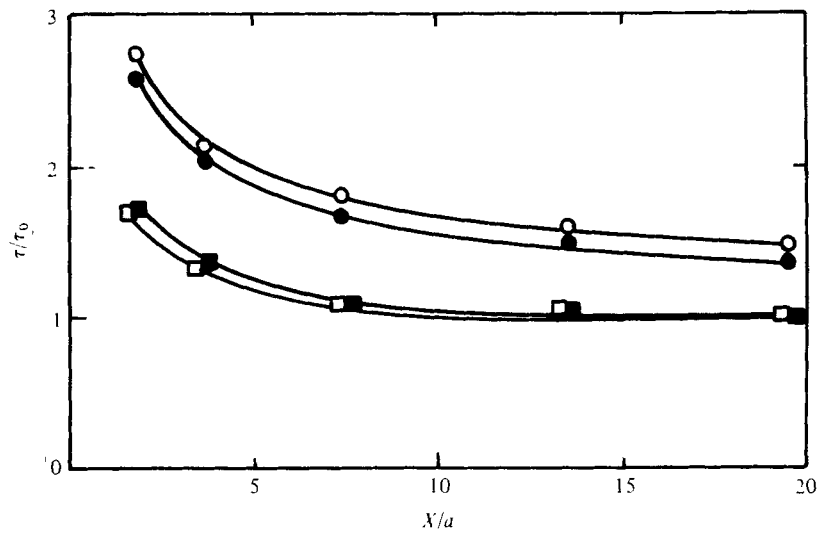

FIGURE 5. Calibration in entry flow in a straight tube. Experimental: ●, Re = 1701; ■, Re = 366. Langhaar (1942): ○, Re = 1701; □, Re = 366.

data is lower by 8 % than theoretical values for the higher flow rate, which is about the same discrepancy found in the fully developed flow comparisons. Thus the accuracy of the electrochemical technique was estimated to be such that the local wall shear rate could be determined in an accuracy of about 7–8 %. The data obtained for fully developed and developing flows in a straight tube indicated that the circumferential distribution of wall shear is uniform at a given section (and also along the length of the tube for fully developed flow) with maximum scatter of ± 4 %.

4.2. *Steady entry flow in a curved tube*

In this section experimental results on the wall shear in the entry region of a curved tube of radius ratio $a/R = \frac{1}{7}$ are presented. The experiments were performed for a wide Dean number range between 139 and 2868.

Circumferential distribution of wall shear stress and its characteristics. The circumferential variations of wall shear stress with Dean number are shown in figures 6 (*a–e*). The wall shear stress is normalized to the fully developed value τ_0 in the corresponding Poiseuille flow at the same Reynolds number. Filled symbols in the figures represent measurements in conventional laminar flows, i.e. for a Reynolds number range between 366 and 1701 (κ = 139 to 643). (The term 'conventional' is used to describe flows at Reynolds numbers less than the critical value of 2000 for transition to turbulence in a straight tube.) Open symbols are used for Reynolds numbers from 3402 to 7588 (κ = 1286 to 2868). The data for high flow rates will be discussed in detail later.

As would be expected in the upstream regions of the bend (sections 1 and 2) the distribution of wall shear is fairly uniform in θ, particularly for lower Dean number flows, as shown in figures 6 (*a, b*). However, as the Dean number is increased, it is observed that the maximum shear stress occurs at about θ = 60°, and thereafter decreases almost linearly toward the outer wall (θ = 180°). This wall shear profile in the upstream region is quite opposite to that of the fully developed region and suggests

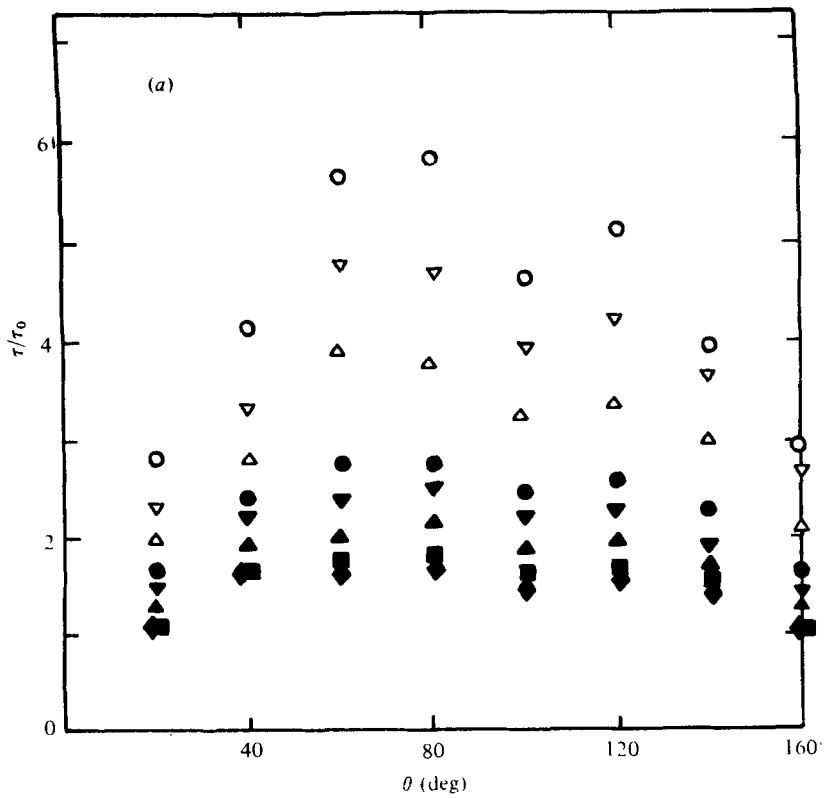

FIGURE 6(a). For legend see p. 478.

that a potential vortex flow is formed in the core of the upstream region. More evidence for the potential vortex flow will be given with reference to Singh's theory (1974). Further downstream, particularly at section 3, the profile has developed a 'valley' (figure 6c) and the local maximum shear stress is achieved at 80° and a second maximum of almost equal strength is obtained at 120°. The existence of a valley in the shear stress profile and the fact that the point of maximum wall shear occurs on the middle portion of the bend (at around 80°) are prominent characteristics of the entry flow in curved tubes. The two peaks in the wall shear profile are indicative of the strong effect of secondary flow. Flow visualization studies on the curved tube suggest that there might be additional pairs of vortices in the entry region. Velocity measurements by Agrawal *et al.* in the same curved tube appear to confirm the existence of such a vortex structure. Figure 7 shows two regions of maximum wall shear rates at section 3. The corresponding isovelocity contours obtained by Agrawal *et al.* ($\kappa = 565$) are superposed for comparison and the location of the conjectured vortices are shown for possible interpretation of the nature of the valley. The flow visualization studies suggested that the inner vortex pair moves away from the centre of curvature and away from the central plane as it grows. The shift may be due to rapid boundary layer growth on the inner portion of the bend. At section 3, this inner vortex pair may cause a second maximum in axial velocity to take place near the region of inner peak wall shear. The inner peak wall shear may then be due to this second maximum axial

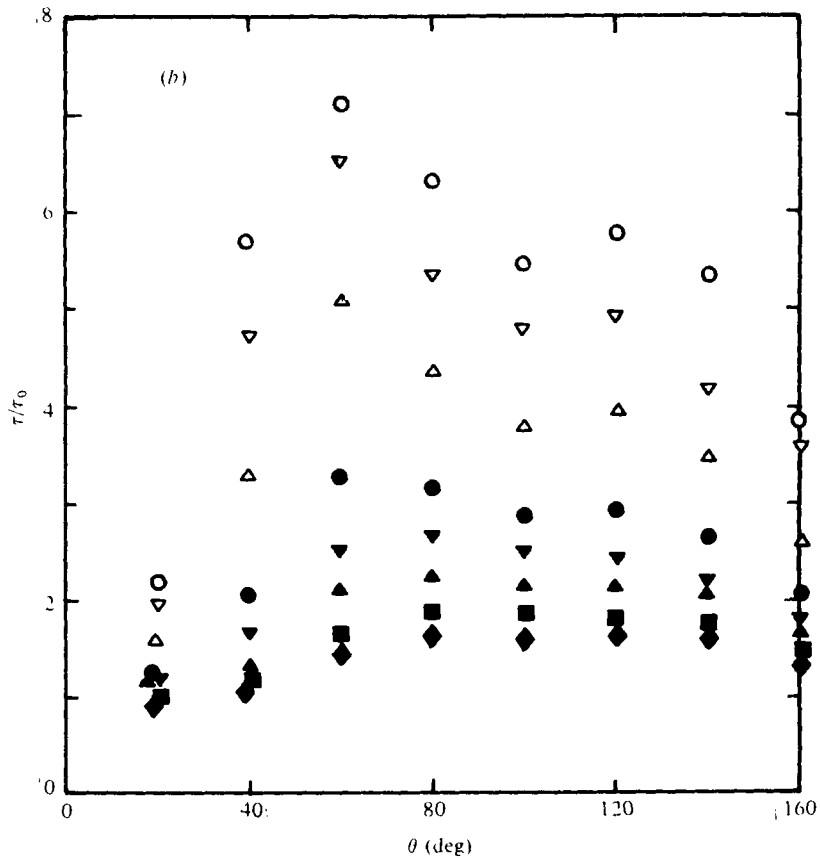

FIGURE 6(*b*). For legend see p. 478.

velocity. The region of maximum axial velocity is shown to be close to the region of outer peak wall shear (figure 7). Farther downstream (figures 6*d* and *e*), the valley in the circumferential wall shear distribution becomes less distinct and moves toward the outer part of the bend. At the last section (figure 6*e*), the profile looks almost fully developed at least in shape, i.e. the wall shear increases toward the outer wall and the maximum wall shear occurs near the outer wall.

The circumferential wall shear distributions normalized to Poiseuille and average values, at different axial locations for a representative Dean number, $\kappa = 643$, are replotted in figures 8 and 9. Wall shear values are lowest at the innermost wall and greatest on the middle portion of the bend as shown in the figures. At a given cross section the wall shear may vary by ratio of 4:1, maximum:minimum, or by ratio of 1·5:1, maximum:average, in the range of Dean numbers studied. The location of maximum and minimum wall shear for the different axial stations are indicated in figure 10, for $\kappa = 643$. These locations seem to remain essentially independent of Dean number, at least over the range of κ investigated. The point of maximum wall shear occurs at $\theta = 60°$ at section 1 and moves outward as flow develops. This shift may be due to shift of maximum axial velocity as observed by Agrawal *et al.* However, the point of minimum wall shear remains on the innermost part of the bend.

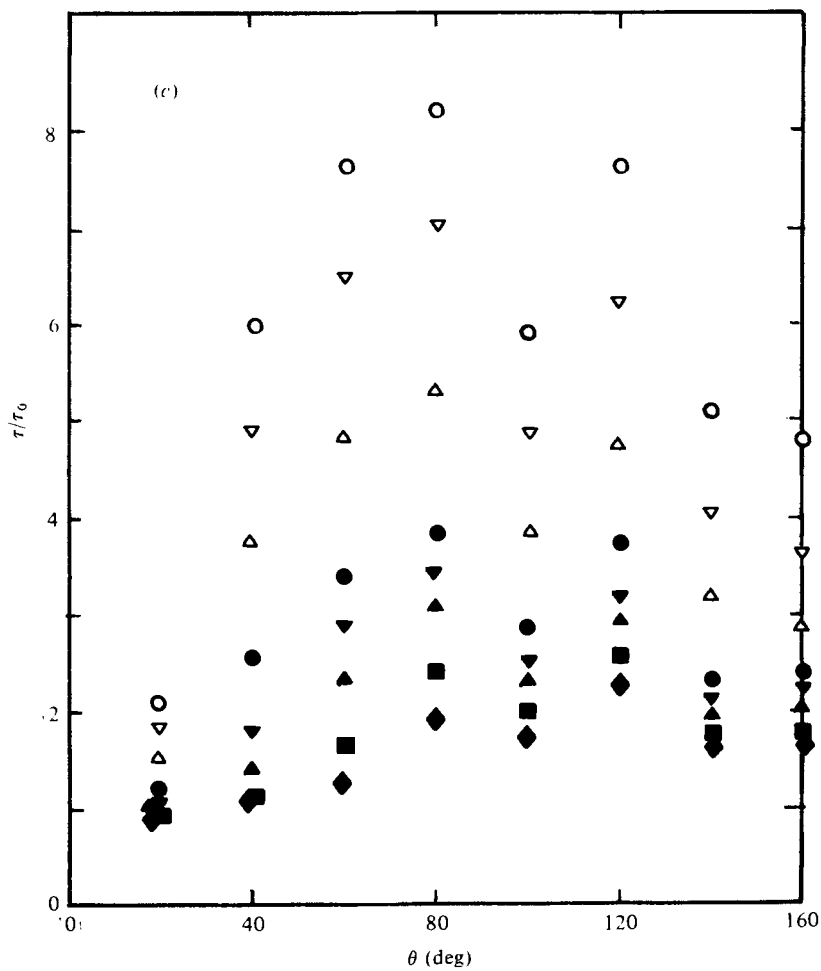

FIGURE 6(c). For legend see p. 478.

Axial distribution of wall shear stress and its characteristics. The variation of shear stress with axial distance is shown for a representative Dean number ($\kappa = 643$) in figure 11. It is seen that the wall shear on the inside portion of the bend decreases with downstream distance while that on the outside increases. This is expected because the boundary layer grows rapidly at the inside wall and does not grow or perhaps decreases in thickness at the outside due to the secondary flow. On the middle portion of the bend the wall shear increases with axial distance up to about four diameters and then decreases slightly. It can be seen in figure 11 that the wall shear stress at the middle portion of the bend rises to about four times the Poiseuille flow value. The θ-averaged wall shear, also plotted in figure 11, shows a non-monotonic variation with axial distance. It is clear that the secondary flow is responsible for this non-monotonic variation. A non-monotonic variation of the heat transfer coefficient with axial distance was also observed in the study of the thermal entrance regions of helically coiled tubes by Seban & McLaughlin (1963) but they believed that natural convection might be responsible for it. This variation was however confirmed in the experimental Nusselt number profiles of Dravid *et al.* (1971) and the numerical

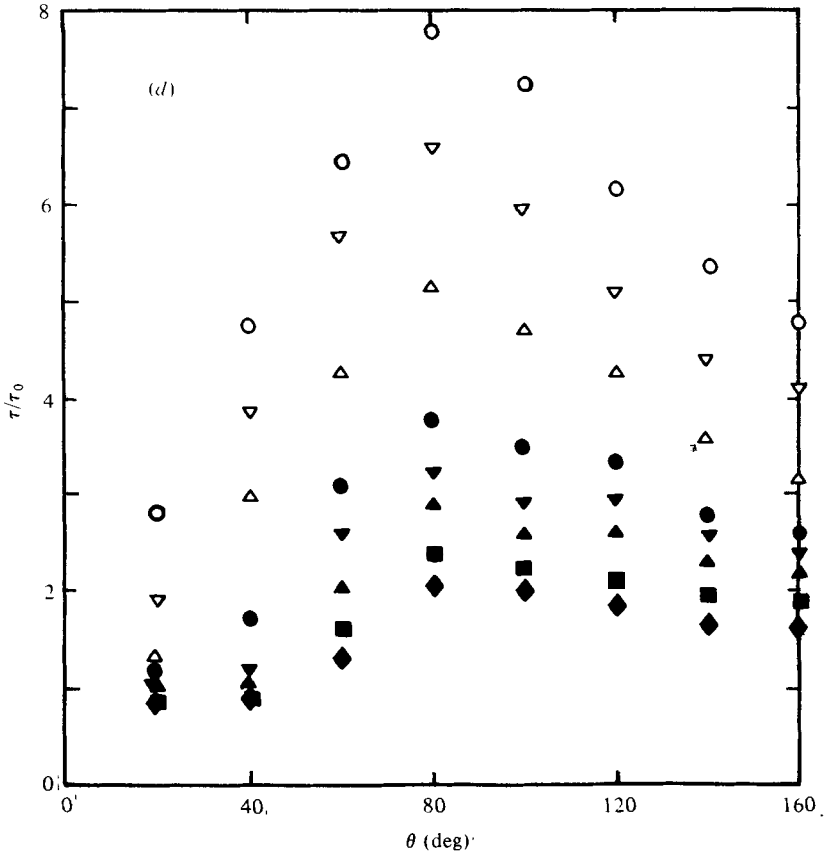

FIGURE 6(*d*). For legend see p. 478.

Nusselt number profiles of Patankar *et al.* (1974) for fluids with low Prandtl number. It is also observed from a comparison between figures 11 and 5 that the θ-averaged wall shear is about the same as the corresponding straight tube value at section 1 but it becomes higher than the straight tube value farther downstream. Thus, it may be said that the secondary flow in the entry region of curved tubes causes a slight increase in wall shear in the upstream region and a large increase in the downstream region in comparison with the straight tube value with the result that a fairly uniform axial distribution of average wall shear is produced.

An estimate of wall shear stress from LDV measurement. Direct comparison between the present results and those of other investigators is not possible because of the lack of experimental data for the entry region of the curved tube. However, the velocity profiles measured by Agrawal *et al.* can be used to estimate the local wall shear; sections 1, 3 and 5, at Dean numbers 184 and 372 were chosen for comparison. For each section the velocity gradients were evaluated at the eight circumferential positions of the tube where electrochemical probes were embedded. To obtain the velocity gradient at each circumferential position, velocity data were interpolated on a computer at four radial positions of 0·0635, 0·1270, 0·1905 and 0·2540 cm from the wall and a plot of axial velocity *vs.* distance from the wall was drawn. A linear axial velocity boundary layer (usually between the wall and the first position of measured

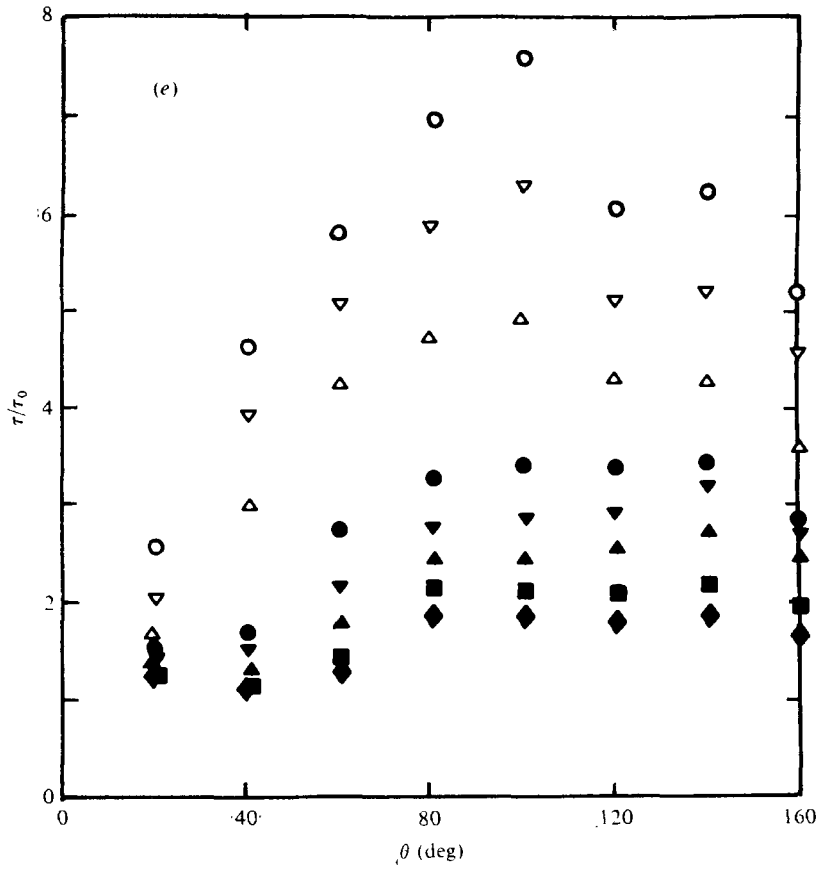

FIGURE 6. Circumferential variation of shear stress. (*a*) $X/a = 1{\cdot}84$; (*b*) $X/a = 3{\cdot}68$; (*c*) $X/a = 7{\cdot}34$; (*d*) $X/a = 13{\cdot}44$; (*e*) $X/a = 19{\cdot}54$. κ values: ◆, 139; ■, 184; ▲, 279; ▼, 372; ●, 643; △, 1286; ▽, 1978; ○, 2868.

velocity at 0·15 cm from the wall) was assumed. The contribution of the secondary velocity gradient was not considered because the secondary velocities were measured at different values of Dean number and at different positions.

The results are shown in figures 12(*a–c*). Although the trends are similar, it appears that the agreement between the experimental and the velocity-gradient-estimated wall shears is not good, especially on the middle portion of the bend. However, it should be remembered that the estimated data represent only the axial velocity component since secondary velocity contributions were neglected. Thus, the discrepancy might reasonably be expected to represent the contribution of the secondary flow to the wall shear. The difference between experimental and estimated wall shears is the largest on the middle portion of the bend, as would be anticipated because the maximum secondary velocity occurs there. The agreement in each section is generally good on the inner and outer portions of the tube where the secondary velocity tends towards zero because of symmetry. Furthermore, the agreement is better for the lower Dean number indicating that the effect of secondary flow is smaller for the lower Dean number as it should be.

Figure 12 provides us with an estimate of the contribution of the secondary flow

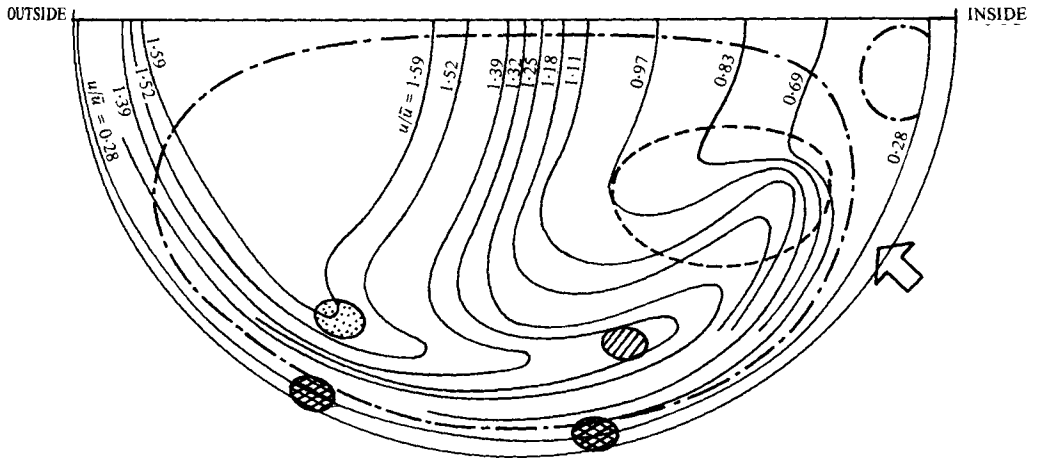

FIGURE 7. Distributions of velocity and shear stress at $X/a = 7{\cdot}34$. Double cross-hatched regions indicate the locations of maximum wall shear stress found in the present study, for $\kappa = 643$. For comparison the isovelocity contours obtained by Agrawal *et al.* (1978) at $\kappa = 565$ are shown (solid line). The stippled and shaded regions indicate the locations of maximum and second maximum axial velocity, and the arrow locates the point on the wall where separation of the secondary flow is believed to have occurred. The region bounded by the –·– curve contains the major portion of the secondary motion, and the region bounded by the – – – curve contains what appeared to be an inner vortex region.

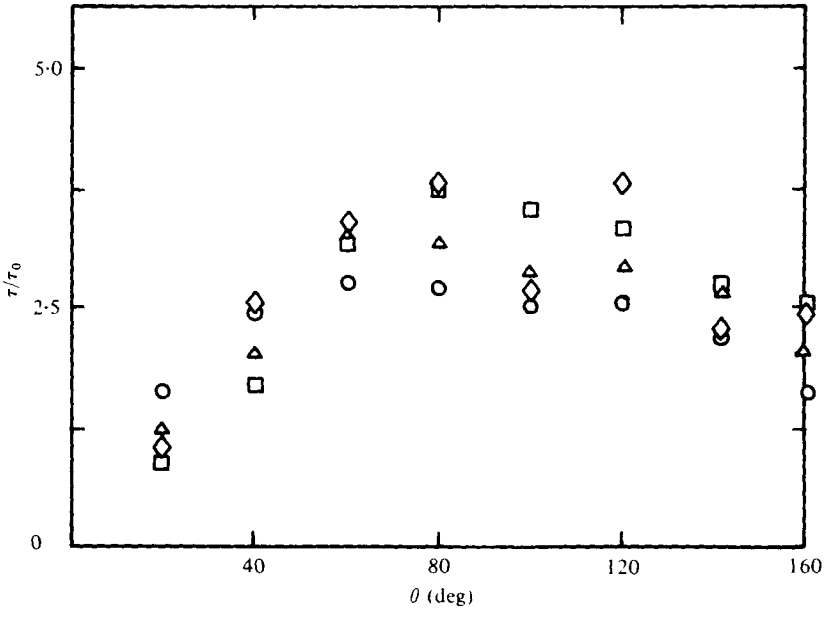

FIGURE 8. Circumferential and axial distributions of shear stress, normalized to the value in the corresponding Poiseuille flow. $\kappa = 643$. X/a values: ○, 1·84; △, 3·68; ◇, 7·34; □, 13·44.

to the total wall shear, since $\tau/\tau_0 = (\tau_{\text{axial}}^2 + \tau_{\text{secondary}}^2)^{\frac{1}{2}}/\tau_0$, where τ is the total wall shear as measured by the electrochemical method, and τ_{axial} is the shear stress inferred from the axial velocity measurements. For $\kappa = 372$, the ratio of $\tau_{\text{secondary}}:\tau_{\text{axial}}$ is estimated to be as high as about 0·6 at $\theta = 80°$ in the entry region. It is interesting to note that Collins & Dennis (1975) have computed a value of about 0·7 at the same θ

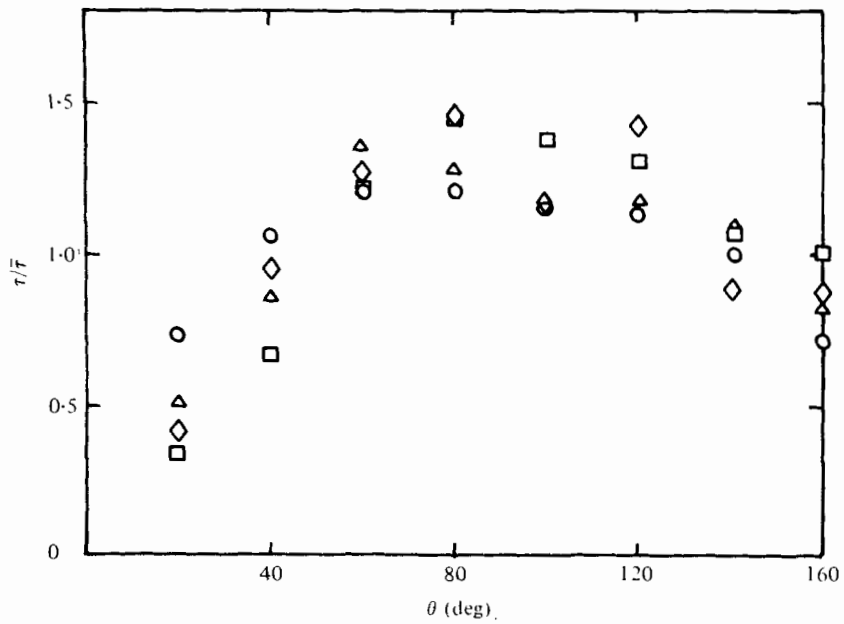

FIGURE 9. Circumferential and axial distributions of shear stress, normalized to the average value over the circumference of each section. $\kappa = 643$. X/a values as in figure 8.

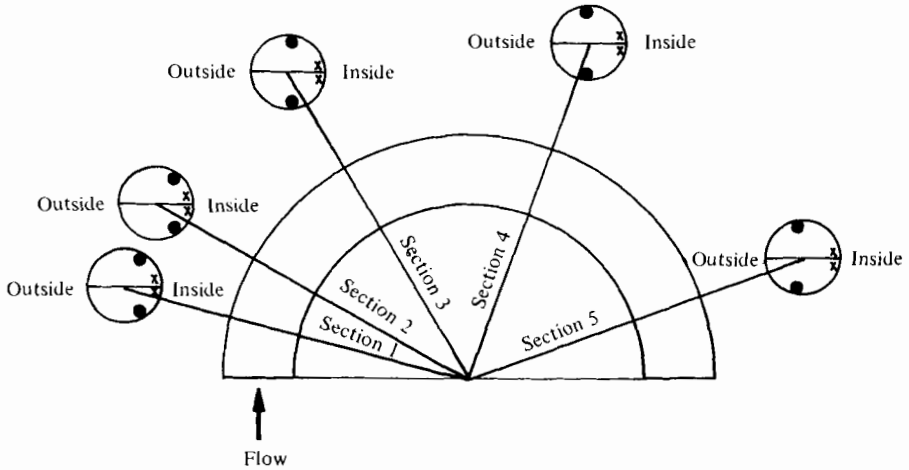

FIGURE 10. Locations of regions of maximum and minimum wall shear stress at the different axial stations. × denotes the location of minimum values, and ● denotes the location of maximum values.

in the fully developed region, so that ratio $\tau_{\text{secondary}}:\tau_{\text{axial}} \approx 0{\cdot}6$ appears reasonable.

It is very interesting to notice particularly in figure 12(*b*) that the velocity-estimated wall shear also exhibits the valley in the middle portion of the bend at section 3, and also indicates that the point of maximum shear stress occurs in this region. The distributions at section 5 as seen in figure 12(*c*) show that for $\kappa = 372$ estimated wall shear rates increase with θ but the data are more uniform on the outer half of the bend.

Comparison with theoretical results. The experimental wall shear distribution is

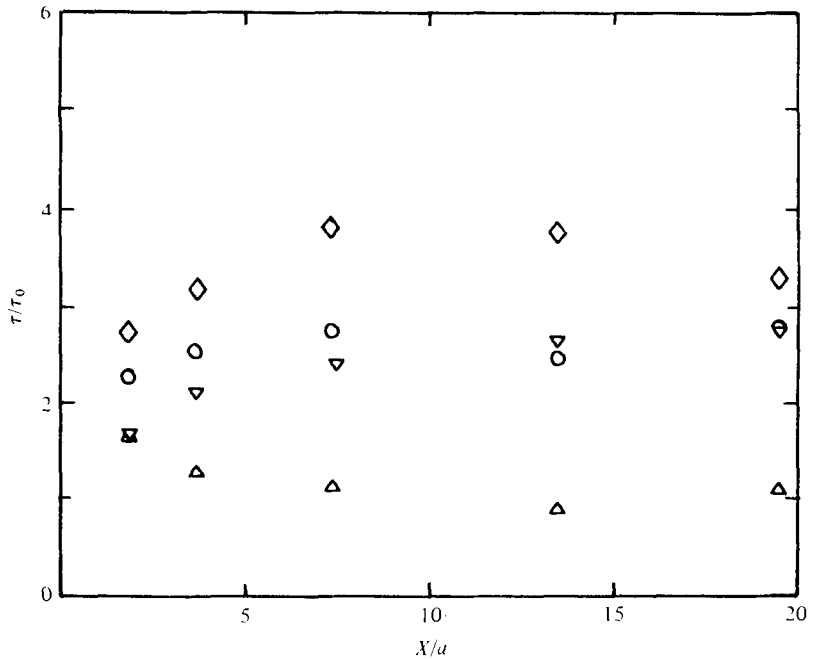

FIGURE 11. Development of shear stress with axial distance. $\kappa = 643$. △, inside, $\theta = 20°$; ◇, middle, $\theta = 80°$; ▽, outside, $\theta = 160°$; ○, average over the circumference of each section.

compared with the theoretical distribution of Singh (1974) in figure 13. At 1·84 radii downstream from the entry plane the agreement between theory and experiment is very good. The theoretical profile begins to diverge from the experimental one at $X/a = 3{\cdot}68$ and at $X/a = 7{\cdot}34$ (not shown) Singh's analysis completely fails to show the existence of a valley. This is not surprising, since Singh's solution is valid only for distances from the inlet smaller than $O(aR)^{\frac{1}{2}}$, which in the present case is equal to $\sqrt{7}a$.

However, it is of interest to compare the location of the cross-over point which is the axial distance from the entrance at which the wall shear stress on the inner side of the bend becomes equal to that on the outer side. The location of the cross-over point was determined by using the experimental data at $\theta = 20$ and 160° and assuming that the data represent the wall shears at $\theta = 0$ and 180°. The location of the cross-over point is shown in figure 14. The cross-over occurs approximately at $X/a = 1{\cdot}96$ while the theoretical value predicted by Singh is 1·90 for the vortex entry condition. It is very interesting to note that our experimental data is closer to the Singh's theoretical result for the vortex entry case than for the uniform entry case. In our experiments, the velocity was uniform at the entrance to the curved tube. But immediately downstream of the entry a transition of the inviscid axial velocity from a uniform velocity distribution to a vortex-type distribution occurs and an almost fully developed vortex-type inviscid core is observed at the first section, $X/a = 1{\cdot}84$ (Agrawal *et al.* 1978). Also, in the present experiment the maximum shear stress was observed near the inner wall and the wall shear decreased toward the outer wall in the upstream sections as mentioned earlier. Thus, it is evident that a potential vortex flow is formed in the core of the upstream region.

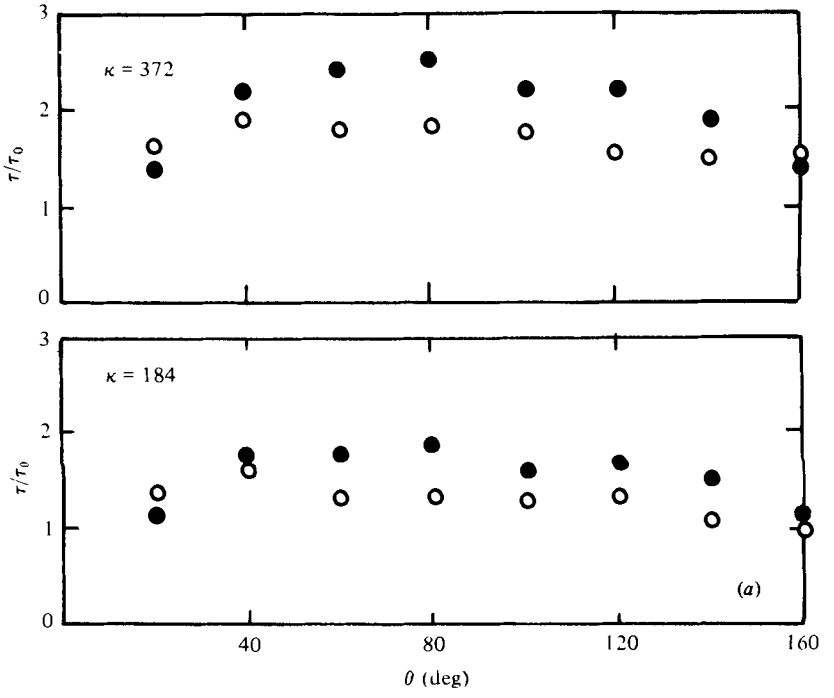

FIGURE 12(*a*). For legend see facing page.

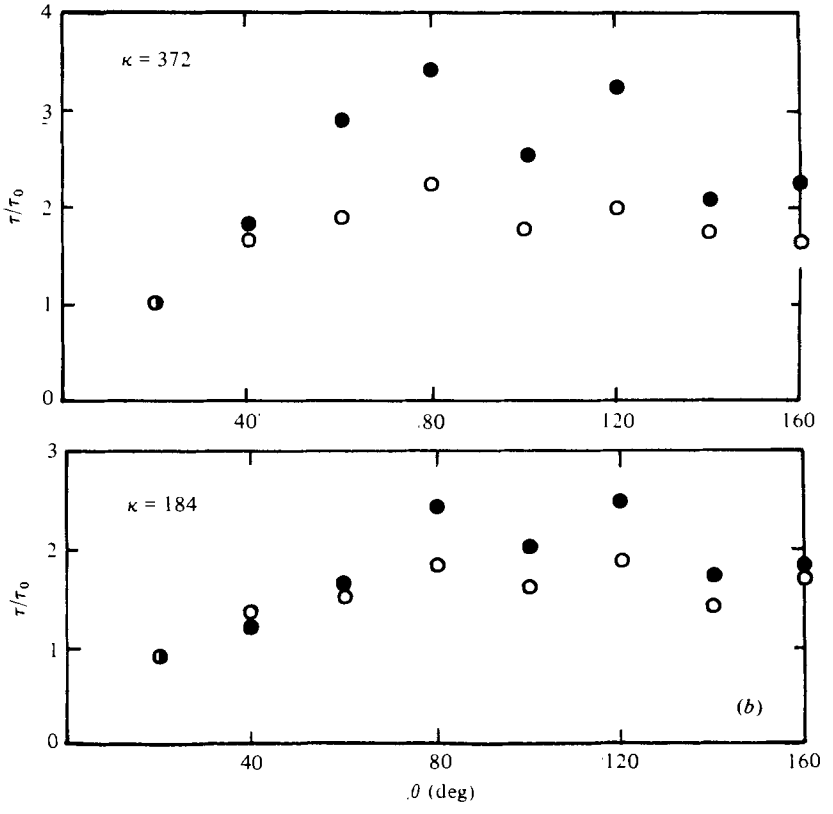

FIGURE 12(*b*). For legend see facing page.

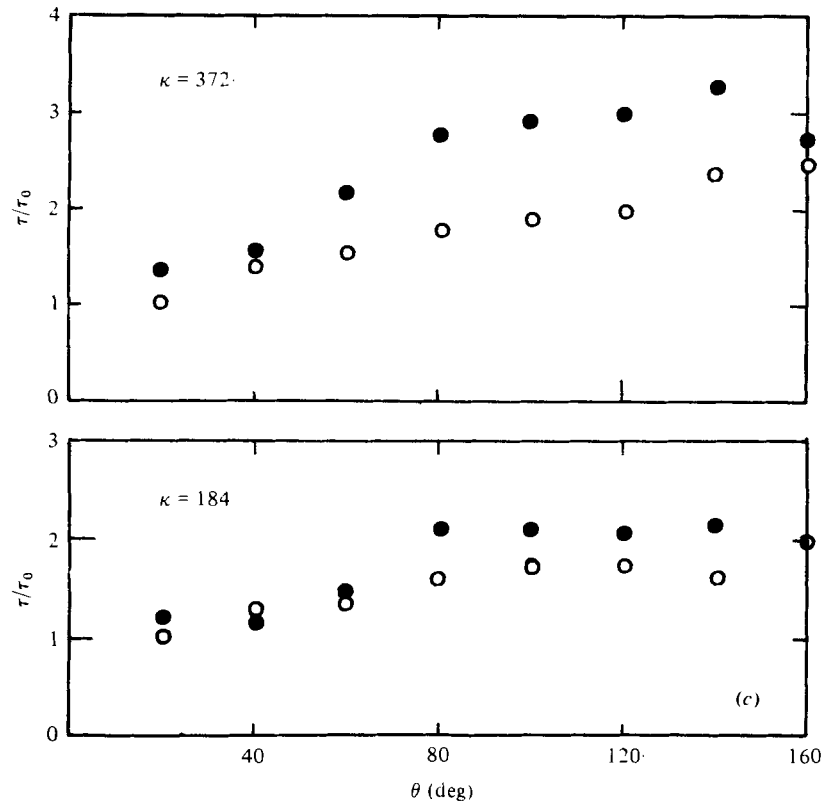

FIGURE 12. Comparison of experimental shear stress with estimated shear stress. (*a*) $X/a = 1{\cdot}84$; (*b*) $X/a = 7{\cdot}34$; (*c*) $X/a = 19{\cdot}54$. ●, present experiments; ○, estimated from Agrawal *et al.* 1978.

The distance from the entry of the cross-over is approximately independent of *Re* as Singh predicted, although the experiments seem to indicate that it may decrease slightly as Reynolds number increases.

Comparison with numerical results. The wall shear stress in fully developed flow in a curved tube was computed for $\kappa = 190{\cdot}9$ and $369{\cdot}5$ from the numerical results of Collins & Dennis (1975)† and is compared with the present measurements at section 5, the farthermost downstream section. It is seen from figure 15 that the agreement is good on the inner part of the tube but there are significant differences over the rest of the circumference. Although the axial velocity profile on the plane of symmetry has been described as similar to the fully developed one (Agrawal *et al.*), the comparison of wall shear stress confirms that the flow is far from fully developed at section 5. According to the theoretical results of Yao & Berger (1975) the entry length for the curved tube for $\kappa = 372$ is about five times greater than the axial distance from the entry to section 5 ($X/a = 19{\cdot}54$). Thus, in the present experiments the entry flow regime extended throughout the whole test section, as in fact it does in the aorta. Further development of flow in the final stages of flow development after section 5 would be expected to change shear stress profiles, mainly on the middle and outer

† The actual numerical results used here are not contained in the 1975 paper, but were very kindly computed subsequently by Prof. Dennis at our request.

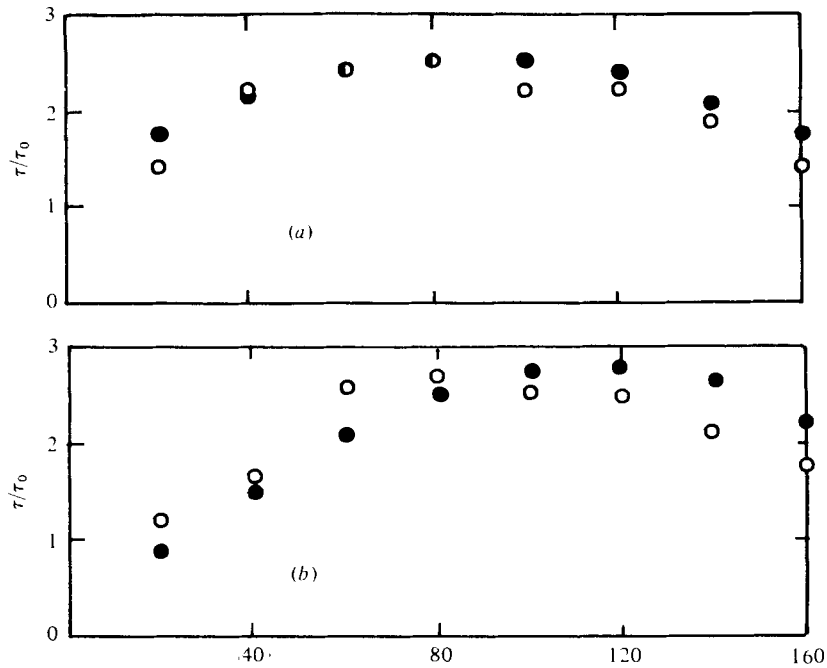

FIGURE 13. Comparison of experimental shear stress with theoretical predictions, for $\kappa = 372$. (*a*) $X/a = 1{\cdot}84$. (*b*) $X/a = 3{\cdot}68$. ○, present experiments; ●, theoretical predictions of Singh (1974).

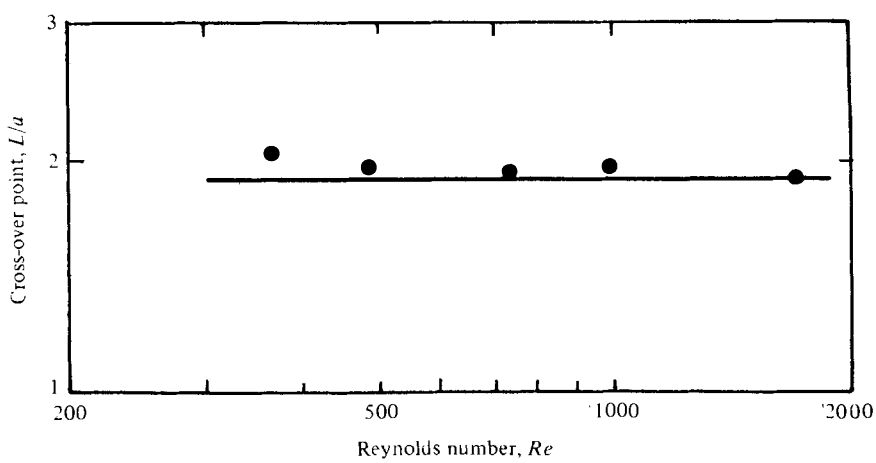

FIGURE 14. Location of the cross-over point. ●, present experiments; ——, Singh (1974).

parts of the tube, so that the peak wall shear which occurs on the outer portion of the bend at $\theta \approx 140°$ might be expected to rise to the fully developed value of Collins & Dennis as shown in figure 15. Thus, the effect of secondary flow on the distributions of velocity, shear stress and mass transfer rates for curved tube flows is expected to be still significant downstream of section 5.

Comparisons were also made between our θ-averaged shear stress ratioed to the Poiseuille value at the furthermost downstream station, $X/a = 19{\cdot}54$, and values of

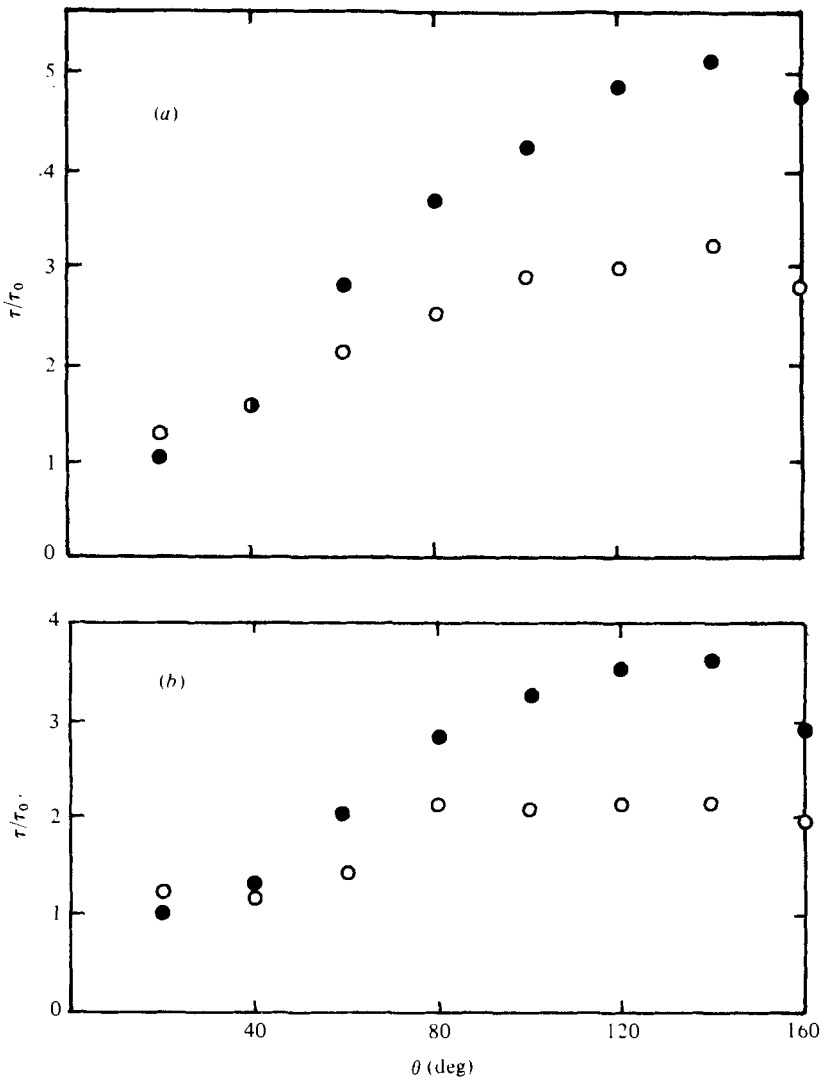

FIGURE 15. Comparison of shear stress profiles in the entry region at $X/a = 19{\cdot}54$ with the fully developed flow. (*a*) ○, $\kappa = 372$, present experiments; ●, $\kappa = 369{\cdot}5$, Collins & Dennis (1975). (*b*) ○, $\kappa = 184$, present experiments; ●, $\kappa = 190{\cdot}9$, Collins & Dennis (1975).

$\bar{\tau}/\tau_0$ calculated by Van Dyke (1978), which in his notation is λ_{cl}/λ_s. Our data fall on Van Dyke's calculated curve (his figure 8) up to a value of κ of about 643, and lie above his curve, a little below the Hasson correlation, for higher values of κ up to our maximum value of 2868. Whether this indicates a discrepancy between theory and experiment is difficult to say, since the flow at the higher values of κ was very likely not fully developed at $X/a = 19{\cdot}58$, and it is not unreasonable to suppose that τ/τ_0 would exceed its fully-developed value in the developing-flow regime.

It should be pointed out that all the analyses both analytical and numerical, which rely on a single parameter, the Dean number, to characterize the flow, apply only to tubes of small curvature since in the full equations of motion the two parameters

$\alpha = a/R$ and $Re = 2u_0 a/\nu$ appear separately. Only for small values of α, when certain terms in the equations can be neglected, do they combine to give the single parameter $\kappa' = Re\sqrt{\alpha}$. Thus in general one expects that both fully developed and developing flows in tubes of arbitrary curvature ratio α will have a functional dependence on both Re and α. Whether in the present experiments the value $\alpha = \frac{1}{7}$ is 'small' enough that a single parameter κ' (or κ) can characterize the flow is difficult to say. The axial velocity profiles obtained by Agrawal *et al.* at comparable values of κ', with $\alpha = \frac{1}{7}$ and $\alpha = \frac{1}{20}$, exhibit significant similarities, but also some discrepancies which may be real or may be due to experimental error. Specific α dependence would be expected to be more prominent in the secondary motion, but unfortunately we have at present accurate secondary velocity data only for $\alpha = \frac{1}{7}$.

The stabilizing effect of secondary flow in a curved tube. Some of the experimental conditions corresponded to Reynolds numbers greater than the value $Re \approx 2000$ associated with transition to turbulence in a straight pipe. These are identified by the open symbols in figures 6(*a–e*). ($Re = \sqrt{7}\kappa$ for these data). Turbulence was expected to occur at these high Reynolds numbers, but no appreciable change was observed in the nature of wall shear distribution, although a valley appeared earlier at section 1 and deepened with downstream distance up to section 3. The early appearance of the valley suggests that the effect of the secondary flow might even be felt upstream of the tube entrance when the Dean number is high, in which case the velocity distribution would no longer be uniform. This however is only conjecture, since the inlet flow was not directly measured.

White (1929) and Taylor (1929) have shown that there is an increase in critical Reynolds number with a/R for curved tubes. Extrapolation of their data shows that the critical Reynolds number is about 7600 for $a/R = \frac{1}{7}$, the value of the present experiments. Thus, we can conclude from our data profiles and Taylor's criterion that most of the flows in our experiments were indeed laminar and the flow at the maximum Reynolds number of our experiments, $Re = 7588$, might still have been laminar. However, random fluctuations in the limiting currents were observed at $Re = 7588$ and this may have indicated the onset of turbulence, but this possibility was not further investigated. The stabilizing effect of secondary flow manifested by the increased critical Reynolds number in our experiments as well as those of White & Taylor may also have been observed in the canine experiments of Nerem, Seed & Wood (1972) where it was found that disturbances occurring in the ascending aorta disappeared in the descending aorta, although comparisons are difficult because in these latter experiments the flow was pulsatile and the vessel non-rigid.

Some physiological considerations. The mechanisms responsible for development of atherosclerosis are not yet completely understood. There are many theories, biochemical and physical, concerning the way in which atheromatous deposits form and much physiological and clinical data exist. It has been hypothesized that wall shear stress may play a role in the focal distribution of vascular lesions, and there are conflicting views as to whether the preferential sites might be regions of high shear or low shear. Since the possibility exists that there is a correlation between the distributions of lesions and wall shear stress, it is of interest to examine our experimental results in respect to this possible correlation.

Our experimental measurements in steady flow in the entry region of a curved tube show that the lowest shear stresses occur along the inner curve region and highest

ones occur along the middle part of the circumference of the bend. The formation of arterial wall plaques and fatty streaks generally occurs also on the inner walls of curved vessels (Mitchell & Schwarz 1965). Thus our experimental data would suggest that the distribution of lesions correlates more with regions of low shear rates, as proposed by Caro *et al.* (1971), than with regions of high shear. The present experiments were carried out in a rigid tube without branches. The actual aortic arch has branches and also the wall of the aorta is not rigid. Moreover the flow in the aorta is pulsatile, with peak velocities as much as ten times the time-averaged mean. Therefore, our observation that regions of low shear appear to correlate positively with the locales for atheromatous lesions can be hardly more than speculative until the effects of branching; wall distensability and flow pulsatility are accounted for. It might be the case that these effects will not substantially alter the observation on the correlation. Only a small fraction (about 20 %) of the total flow in the aorta goes to branches in the arch region and as such may not cause a large change in the flow pattern in the inner region of the bend. The radius of an arterial blood vessel does not change more than about 5 % during the cardiac cycle (McDonald 1974) and thus conclusions drawn from rigid tube experiments should still be valid for the aorta (Lighthill 1972). Finally, pulsatile flow may not change appreciably the location of the low shear regions because the location seems to remain unchanged with flow rate as our experiments have indicated, although this conjecture remains to be confirmed by experiments in pulsatile flows.

It may be interesting to note that flow separation may be another candidate of flow phenomena for the causation of atherogenesis. Fox & Hugh (1966) explained the locations of atheroma based on boundary layer separation. Rodkiewicz (1975) postulated from *in vivo* testing and aorta model studies that the atherosclerotic formations in the aortic arch commence and develop at the locations where there are separation and stagnation regions present. The regions of atherosclerotic formation on the inner portion of the bend shown in his paper correspond to approximately sections 2–5 of the curved tube used in this study. Agrawal *et al.* have also indicated that separation of the circumferential boundary layer (though not of the axial flow) may have occurred on the inner portion of the bend from section 3 up to section 5 for $\kappa = 138$ and between sections 4 and 5 for $\kappa = 678$. Therefore, it is possible that the development of atherosclerosis may be facilitated by three-dimensional boundary layer separation.

Narem *et al.* (1972) have speculated that turbulence or random fluctuations might occur at the peak systolic velocity in the human aorta. However, Ling *et al.* (1968) and Schultz *et al.* (1969) have reported that turbulence is an occasional phenomenon occurring in smaller animals only. From direct velocity measurements using a heated film probe Schultz *et al.* have observed virtually undisturbed flow in humans at peak Reynolds numbers as high as 7800. The stabilizing effect of vessel curvature under steady flow conditions has been demonstrated in our experiment at Reynolds numbers as high as 7588. The absence of turbulence at peak Reynolds numbers well above the value for transition in steady flow in straight pipes as observed by Schultz is very likely due to a combination of curvature and pulsatile effects.

5. Conclusion

Local wall shear rates in steady flow in the entry region of a curved tube have been determined using small probes mounted flush with the wall of a rigid curved tube and measuring the mass-transfer-limited currents for the reduction of ferricyanide ions. The experiments were performed for a range of Dean numbers between 139 and 2868.

Calibration experiments have shown that the local wall shear rates can be determined to an accuracy of 7–8 %. The experiments have revealed that secondary flows have a significant influence on the wall shear distributions as well as on the flow development. The principal results can be summarized as follows.

(1) A significant feature of the entry flow in a curved tube is the existence of a valley in the circumferential wall shear distribution in the region of the middle of the bend. The two peaks of wall shear which bound the valley suggest a vortex structure with several pairs of vortices in the developing curved tube flow, in contrast with one pair in the fully developed curved tube flow.

(2) The wall shear stresses in the entry region of a curved tube have a wide circumferential variation due to the secondary flow. Wall shear is smallest at the innermost part of the bend and largest near the middle of the bend, not at the outer wall. At a given cross-section wall shear rates may vary by ratio of 4: 1, maximum: minimum, in the range of Dean number between 139 and 2868. The wall shear stress is significantly enhanced by the secondary motion in the flow development region. For a Dean number range up to 2868, maximum wall shears observed were up to eight times that for fully developed Poiseuille flow.

(3) The circumferential wall shear profiles in the upstream region, together with the experimental and theoretical values of the cross-over points, suggest that a potential vortex flow is formed in the upstream core.

(4) The wall shear on the inside part of the bend decreases with downstream distance while that on the outside increases. The cross-over occurs approximately at 1·96 radii from the inlet and seems to decrease slightly with Reynolds number. There exists a region where the circumferentially averaged wall shear stress increases with increasing downstream distance, whereas the wall shear stress decreases with axial distance in the entry region of a straight tube. It is concluded that the secondary flow in the entry region of a curved tube causes a slight increase in average wall shear in the upstream region and a large increase in the downstream region such that a more uniform axial distribution of average wall shear is attained in a curved tube than in a straight tube.

(5) The present work suggests that the development of atherosclerosis may be linked with low shear regions, rather than high shear, and may also be facilitated by boundary layer separation. The results of the present work should also be useful in the development of better mathematical models for curved tube flow and in the design of coiled heat exchangers.

This work was supported by the National Institute of Health, under grant no. HL 18298 and subsequently by the National Science Foundation under grant no. ENG73-03970A03. The authors are indebted to Professors S. A. Berger and C. W. Tobias for many helpful discussions. Appreciation is expressed to Prof. S. C. R. Dennis for providing the calculation of wall shear.

REFERENCES

AGRAWAL, Y. C., TALBOT, L. & GONG, K. 1978 *J. Fluid Mech.* **85**, 497.

BELLHOUSE, B. J. & TALBOT, L. 1969 *J. Fluid Mech.* **35**, 721.

CARO, C. G., FITZ-GERALD, J. M. & SCHROTER, R. C. 1971 *Proc. Roy. Soc.* B **177**, 109.

CHOI, U. S. 1978 Experimental study of wall shear rates in the entry region of a curved tube. Ph.D. thesis, University of California, Berkeley.

COLLINS, W. M. & DENNIS, S. C. R. 1975 *Quart. J. Mech. Appl. Math.* **28**, 133.

DEAN, W. R. 1927 *Phil. Mag.* **4**, 208.

DEAN, W. R. 1928 *Phil. Mag.* **5**, 673.

DRAVID, A. N., SMITH, K. A., MERRILL, E. W. & BRIAN, P. L. T. 1971 *A.I.Ch.E. J.* **17**, 1107.

FOX, J. A. & HUGH, A. E. 1966 *British Heart J.* **28**, 388.

FRY, D. L. 1968 *Circ. Res.* **22**, 165.

FRY, D. L. 1973 In *Atherogenesis: Initiating Factors*. Ciba Symposium, vol. 12, p. 93. North Holland: Elsevier, Excerpta Medica.

GORDON, S. L., NEWMAN, J. S. & TOBIAS, C. W. 1965 *Berichte der Bunsengesellschaft für physikalische Chemie* **70** (4), 414.

HAWTHORNE, W. R. 1951 *Proc. Roy. Soc.* A **206**, 374.

HUMPHREY, J. A. C. 1977 Flow in ducts with curvature and roughness. Ph.D. thesis, Imperial College of Science and Technology.

LANGHAAR, H. L. 1942 *J. Appl. Mech.* **9**, A55.

LÉVÊQUE, M. 1928 *Annales des Mines* **13**, 201.

LIGHTHILL, M. J. 1950 *Proc. Roy. Soc.* A **202**, 359.

LIGHTHILL, M. J. 1972 *J. Fuid Mech.* **52**, 475.

LING, S. C., ATABEK, H. B., FRY, D. L., PATEL, D. J. & JANICKI, J. S. 1968 *Circ. Res.* **23**, 789.

MCDONALD, D. A. 1974 *Blood Flow in Arteries*. London: Edward Arnold Ltd.

MITCHELL, J. R. & SCHWARZ, C. J. 1965 *Arterial Disease*. Oxford: Blackwell Scientific Publications.

MIZUSHINA, T. 1971 In *Adv. in Heat Transfer*, vol. 7, (ed. T. P. Irvine & J. P. Hartnett), p. 87.

NEREM, R. M., SEED, W. A. & WOOD, N. B. 1972 *J. Fluid Mech.* **52**, 137.

OLSON, D. E. 1971 Fluid mechanics relevant to respiratory flow within curved or elliptic tubes and bifurcating systems. Ph.D. thesis, Imperial College, London.

PATANKAR, S. V., PRATAP, V. S. & SPALDING, D. B. 1974 *J. Fluid Mech.* **62**, 539.

RODKIEWICZ, C. M. 1975 *J. Biomech.* **8**, 149.

SCHULTZ, D. L., TUNSTALL PEDOE, D. S., LEE, G. DE J., GUNNING, A. J. & BELLHOUSE, B. J. 1969 In *Circulatory and Respiratory Mass Transport*. A Ciba Foundation Symposium (ed. G. E. W. Wolstenholme & J. Knight), London: Churchill, p. 172.

SEBAN, R. A. & MCLAUGHLIN, G. F. 1963 *Int. J. Heat Mass. Transfer* **6**, 387.

SINGH, M. P. 1974 *J. Fluid Mech.* **65**, 517.

SMITH, F. T. 1976 *Proc. Roy. Soc.* A **351**, 71.

TAYLOR, G. I. 1929 *Proc. Roy. Soc.* A **124**, 243.

VAN DYKE, M. 1978 *J. Fluid Mech.* **86**, 129.

WHITE, C. M. 1929 *Proc. Roy. Soc.* A **123**, 645.

YAO, L. S. & BERGER, S. A. 1975 *J. Fluid Mech.* **67**, 177.